

Spectral observations of X Persei: Connection between $H\alpha$ and X-ray emission

R. Zamanov^{1,*}, K. A. Stoyanov¹, U. Wolter², D. Marchev³, and N. I. Petrov¹

¹ Institute of Astronomy and National Astronomical Observatory, Bulgarian Academy of Sciences, Tsarigradsko Shose 72, BG-1784 Sofia, Bulgaria

² Hamburger Sternwarte, Universität Hamburg, Gojenbergsweg 112, 21029 Hamburg, Germany

³ Department of Physics and Astronomy, Shumen University, 115 Universitetska Str., 9700 Shumen, Bulgaria

Received November 1, 2018; accepted January 10, 2019

ABSTRACT

We present spectroscopic observations of the Be/X-ray binary X Per obtained during the period 1999 - 2018. Using new and published data, we found that during "disc-rise" the expansion velocity of the circumstellar disc is $0.4 - 0.7 \text{ km s}^{-1}$. Our results suggest that the disc radius in recent decades show evidence of resonant truncation of the disc by resonances 10:1, 3:1, and 2:1, while the maximum disc size is larger than the Roche lobe of the primary and smaller than the closest approach of the neutron star. We find correlation between equivalent width of $H\alpha$ emission line ($W\alpha$) and the X-ray flux, which is visible when $15 \text{ \AA} < W\alpha \leq 40 \text{ \AA}$. The correlation is probably due to wind Roche lobe overflow.

Key words. Stars: emission-line, Be – stars: winds, outflows – X-rays: binaries – Accretion, accretion discs – stars: individual: X Per

1. Introduction

X Persei (HD 24534) is a relatively bright variable star, detected in X-rays with *UHURU* satellite and identified as the optical counterpart of the pulsating X-ray source 4U 0352+309 (Braes & Miley 1972; van den Bergh 1972). This object belongs to the class of Be/X-ray binaries which contains about 100 confirmed and suspected members in our Galaxy, see e.g. Apparao (1994) and Reig (2011). The main component of X Per is a hot massive rapidly rotating Be star. The secondary is a slowly spinning neutron star ($P_{\text{spin}} \approx 837 \text{ s}$) accreting matter from the wind of the primary component (Maitra et al. 2017). On the basis of data from Rossi X-Ray Timing Explorer, Delgado-Martí et al. (2001) determined the orbital period $\sim 250 \text{ d}$, orbital eccentricity $e = 0.11$, and semi-major axis $a = 2.2 \text{ a.u.}$ X Per is considered prototype of the class of Be/X-ray binaries with long orbital periods and near-circular orbits (Pfahl et al. 2002), also named "low-e BeX" (Negueruela 2004). The low orbital eccentricity may be explained by a supernova explosion at which the neutron star did not receive a large impulse, or "kick," at the time of formation, and all induced eccentricity is due to mass loss. Knigge et al. (2011) suggested that it may be related to the type of the supernovae explosion which produced the neutron star, i.e. core-collapse or electron-capture supernova.

X Per is a low-luminosity persistent X-ray source and periodic X-ray outbursts are not obvious in its X-ray light curve. La Palombara & Mereghetti (2007) and Lutovinov et al. (2012) detected X-ray flares and variability in the X-ray light curve. Maitra et al. (2017) detected variability of the pulse profile and energy spectrum and suggested that it is a result of changes in the accretion geometry. X Per has an unusually hard X-ray spectrum (Worrall et al. 1981). It is confidently detected by INTEGRAL

up to more than 100 keV, which can be explained as a result of the dynamical Comptonization in the accretion flow of photons emerging from the polar cap (Doroshenko et al. 2012).

In the last century, the visual magnitude of X Per varies in the range $V = 6.8$ to 6.2 mag . The brightness variations are accompanied by variations in the intensity of the emission lines. The optical spectrum of X Per shows strong emission in the Balmer lines, when it is brighter than 6.5 mag (Dorren et al. 1979; Telting et al. 1998). The brightness variability is probably connected with various disc-rise and disc-fade events. During the last 50 years, the star exhibited two low states - probably disc-less episodes during 1974-1977 and 1990-1991. Absence of emission lines in 1977 was noted by de Loore et al. (1979). Roche et al. (1993) identified that the low state was during 1974-1977. Dramatic changes were observed in 1990, when X Per lost the $H\alpha$ emission line, infrared excess, and circumstellar disc (Norton et al. 1991). The emission lines disappeared and the optical spectrum was dominated by absorption lines, which is typical for normal early-type star.

We present optical spectroscopic observations obtained in recent decades and discuss the radius of the circumstellar disc, outflowing velocity in the disc, disc truncation, and connection with X-ray emission.

2. Observations

The optical spectra of X Per were secured with the 2.0 m telescope of the Rozhen National Astronomical Observatory, Bulgaria and with the robotic 1.2 m TIGRE telescope located in the astronomical observatory La Luz in Mexico. The Rozhen spectra were obtained with the Coude spectrograph and with the Echelle spectrograph ESpeRo (Bonev et al. 2017). The Coude spectra have dispersion 0.1 \AA px^{-1} or 0.2 \AA px^{-1} , while the Echelle spec-

* e-mail: rkz@astro.bas.bg, kstoyanov@astro.bas.bg

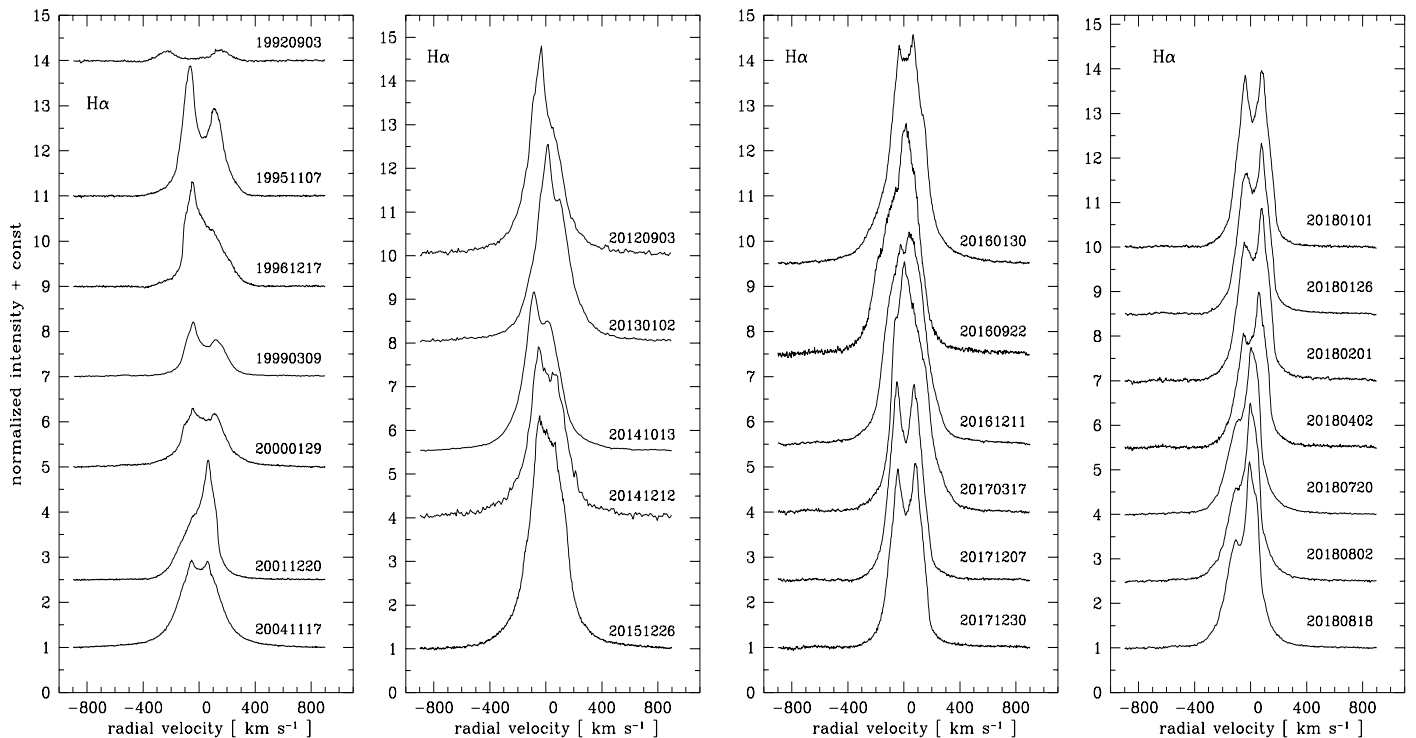


Fig. 1. Variability of $H\alpha$ emission line profile of X Per. The date of observations is in format YYYYMMDD.

tra have 0.06 \AA px^{-1} at 6560 \AA and 0.04 \AA px^{-1} at 4800 \AA . The TIGRE spectra were obtained with the HEROS spectrograph, which provides a spectral resolution of 20000 over the visual spectral range from 3800 \AA to 8800 \AA (Schmitt et al. 2014). A few more spectra were downloaded from the ELODIE archive (Moultaka et al. 2004). These were obtained with the 1.93 m telescope of Observatoire de Haute-Provence.

The measured parameters are given in Table 1. The variability of $H\alpha$ emission line of X Per is presented in Fig.1 (emission line profile), Fig.2 (distance between the peaks), Fig.3 (comparison between two high resolution profiles), Fig.4 (histogram of the $H\alpha$ disc size), and Fig.5 (long term behaviour). During the period 1992 - 2018, the equivalent of $H\alpha$ emission line (W_α) varies from 2 \AA up to 40 \AA . From Fig.1, it is visible that the $H\alpha$ emission line, which exhibits various profile shapes, in some cases is symmetric with two peaks that are well separated, single-peak, double-peak and asymmetric profiles indicating density inhomogeneities.

3. Primary component

3.1. Radius and mass of the primary

From IR observations, Taranova & Shenavrin (2017) obtained temperature $T = 26000 \pm 1000 \text{ K}$ and radius $R_1 = 17.1 \pm 0.6 R_\odot$ for the donor star, adopting distance to the system $d = 1300 \text{ pc}$. GAIA Data Release 2 (Gaia Collaboration et al. 2016, 2018) gives parallax 1.234 mas , which corresponds to a distance 810 pc . With the GAIA distance the results of Taranova & Shenavrin (2017) should give $R_1 = 10.7 R_\odot$.

The B-V and U-B colours of X Per in low state should represent the colours of the primary component. During the period JD 2448545 (1991 October 15) - JD 2449046 (1993 February

27), the brightness of X Per was low $V \approx 6.77$, and the circumstellar disc was very small. At that time the average colours were $(B - V) = 0.09 \pm 0.03$ and $(U - B) = -0.68 \pm 0.03$ (Zamanov & Zamanova 1995). Adopting interstellar extinction towards X Per $E_{B-V} = 0.356$ (Viotti et al. 1982; Nikolov et al. 2017), we calculate dereddened colours $(B - V)_0 = -0.26 \pm 0.03$ and $(U - B)_0 = -0.95 \pm 0.03$. Following Schmidt-Kaler (1982), these colours correspond to B1 III - V spectral type, which is about one spectral type later than B0 derived by Roche et al. (1997) and Lyubimkov et al. (1997), and O9.5III by Fabregat et al. (1992).

Using the well-known formula for the absolute V magnitude, we obtain $M_V = -3.86$. The bolometric magnitude is $M_{bol} = M_V + BC$, where the bolometric correction is $BC = -2.70$ (Schmidt-Kaler 1982; Nieva 2013). Using the solar values $T_\odot = 5780 \text{ K}$ and $M_{bol}^{sun} = 4^m.69$, we calculate $R_1 = 9.2 R_\odot$, which is similar to the above value from Taranova & Shenavrin (2017).

Hohle et al. (2010) give average masses for B0V and B1V stars $15.0 M_\odot$ and $12.0 M_\odot$, respectively. Hereafter for the primary of X Per, we adopt radius $9.2 R_\odot < R_1 < 10.7 R_\odot$ ($R_1 = 10.5 \pm 1.2 R_\odot$) and mass $12.0 M_\odot \leq M_1 \leq 15.0 M_\odot$ ($M_1 = 13.5 \pm 1.5 M_\odot$).

3.2. Rotation of the primary

Dachs et al. (1986) and Hanuschik (1989) established a relation between $v \sin i$, full width at half maximum (FWHM), and W_α of the $H\alpha$ emission line. To calculate $v \sin i$, we use this relation in the form

$$v \sin i = 0.813 (FWHM 10^{0.08 \log W_\alpha - 0.14} - 70 \text{ km s}^{-1}), \quad (1)$$

where FWHM and $v \sin i$ are measured in km s^{-1} , W_α is in [\AA]. We measure FWHM and W_α on our spectra and obtain projected

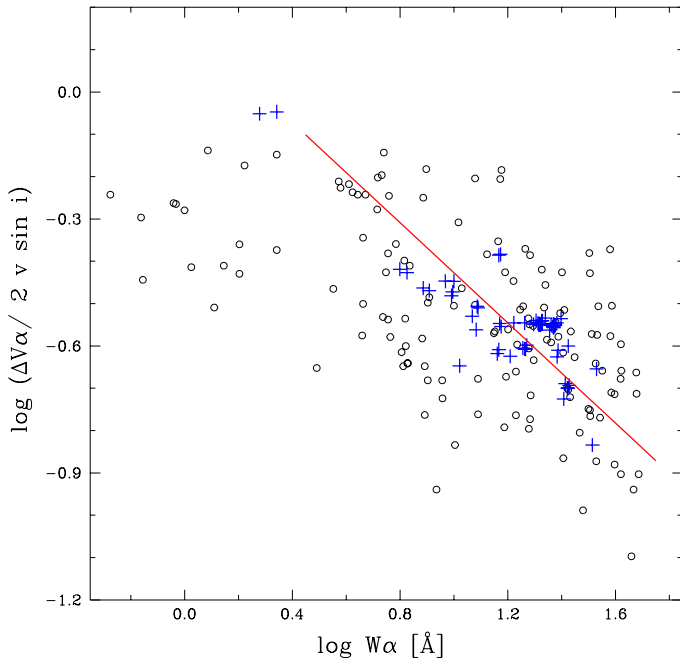


Fig. 2. Distance between the peaks normalized with stellar rotation vs. W_α .

rotational velocity in the range $179 \leq v \sin i \leq 217 \text{ km s}^{-1}$ with average $v \sin i = 191 \pm 12 \text{ km s}^{-1}$. This value is close to that of Lyubimkov et al. (1997), who estimated projected rotational velocity $v \sin i = 215 \pm 10 \text{ km s}^{-1}$ using He I $\lambda 4026 \text{ \AA}$ absorption line.

4. Be disc

In Fig. 2, we plot $\log \Delta V_\alpha / 2v \sin i$ versus $\log W_\alpha$. The black open circles are data for Be stars taken from Andriolat (1983), Hanuschik (1986), Hanuschik et al. (1988), Dachs et al. (1992), Slettebak et al. (1992), and Catanzaro (2013). The blue plus signs are our measurements of X Per. Most of the data points of X Per are in the middle of the Be star populations. The exceptions are two points obtained on 19920903 and 19920905, when the disc was small. Because these points are above the population of other Be stars, following Sect. 5.2 of Hanuschik et al. (1988), this probably indicates that the disc of X Per was denser during the early stages of its development. Later, when the disc is larger, it follows the average behaviour of other Be stars. For X Per we have 15 spectra on which both $H\alpha$ and $H\beta$ emission lines have two peaks (see Table 1). We calculate median value $\Delta V_\beta / \Delta V_\alpha = 1.24$ and average value $\Delta V_\beta / \Delta V_\alpha = 1.30 \pm 0.26$.

The Balmer emission lines form primarily in the disc surrounding the Be star, and the total flux of the feature (measured as the line equivalent width) is closely related to the size of the disc. The discs of the Be stars are Keplerian supported by the rotation (e.g. Porter & Rivinius (2003) and references therein). For a Keplerian circumstellar disc the peak separation can be regarded as a measure of the outer radius (R_{disc}) of the emitting

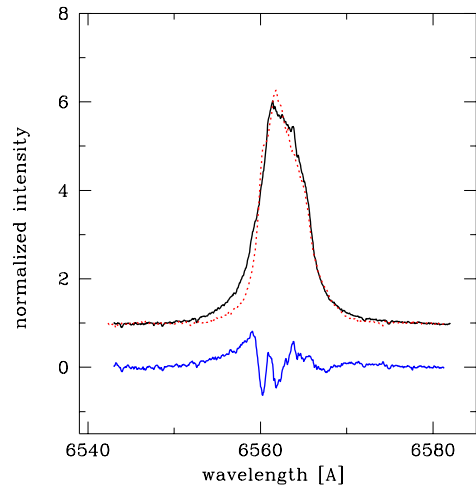


Fig. 3. $H\alpha$ emission line profile of X Per in December 2015 (black solid line) and March 2017 (red dotted line). The two are spectra obtained about one year apart. The difference between the spectra is also plotted and seems to indicate slow outward motion with velocity $\approx 5.1 \text{ km s}^{-1}$ (see Sect. 4.1).

disc,

$$R_{disc} = R_1 \frac{(2v \sin i)^2}{\Delta V^2}, \quad (2)$$

where R_1 is the radius of the primary, $v \sin i$ is its projected rotational velocity. When the two peaks are visible in the emission lines, we can estimate the disc radius using Eq. 2. The disc size is also connected with W_α ,

$$R_{disc} = \epsilon R_1 0.467 W_\alpha^{1.184}, \quad (3)$$

where ϵ is a dimensionless parameter, for which we adopt $\epsilon = 0.9 \pm 0.1$ (see Zamanov et al. (2016), Sect. 4.3). This equation expresses the fact that R_{disc} grows as W_α becomes larger (e.g. Grundstrom & Gies 2006). A slightly different expression for the relation between R_{disc} and W_α is used in Coe et al. (2006) and Monageng et al. (2017).

4.1. Radial outflow velocity

During the period JD 2448869 to JD 2450029 a steady increase of the $H\alpha$ emission is visible (Fig. 5). The equivalent width increased from $W_\alpha = -2.0 \text{ \AA}$ to -14.9 \AA , and the distance between the peaks decreased from $\Delta V = 382 \text{ km s}^{-1}$ to $\Delta V = 177 \text{ km s}^{-1}$. Following Eq. 2 this corresponds to change of the disc radius from $13 R_\odot$ to $62 R_\odot$ and expansion velocity of disc $V_{out} = 0.35 \text{ km s}^{-1}$. Using W_α and Eq. 3 this corresponds to change of the disc radius from $10 R_\odot$ to $108 R_\odot$ and expansion velocity of disc $V_{out} = 0.70 \text{ km s}^{-1}$.

During the period JD 2452800 to JD 2455500 a steady increase of the $H\alpha$ emission is also visible (Fig. 5). The equivalent width increased from $W_\alpha = -12 \text{ \AA}$ to -37 \AA . Using Eq. 3, this corresponds to $V_{out} = 0.67 \text{ km s}^{-1}$.

We compared the high resolution emission line profiles obtained with the ESPERO spectrograph. An interesting result emerged when we compared the $H\alpha$ profiles obtained in December 2015 with that in March 2017 (see Fig. 3). It seems that during this period the material that was emitting in the wings of the $H\alpha$ emission moved to the outer parts of the disc and

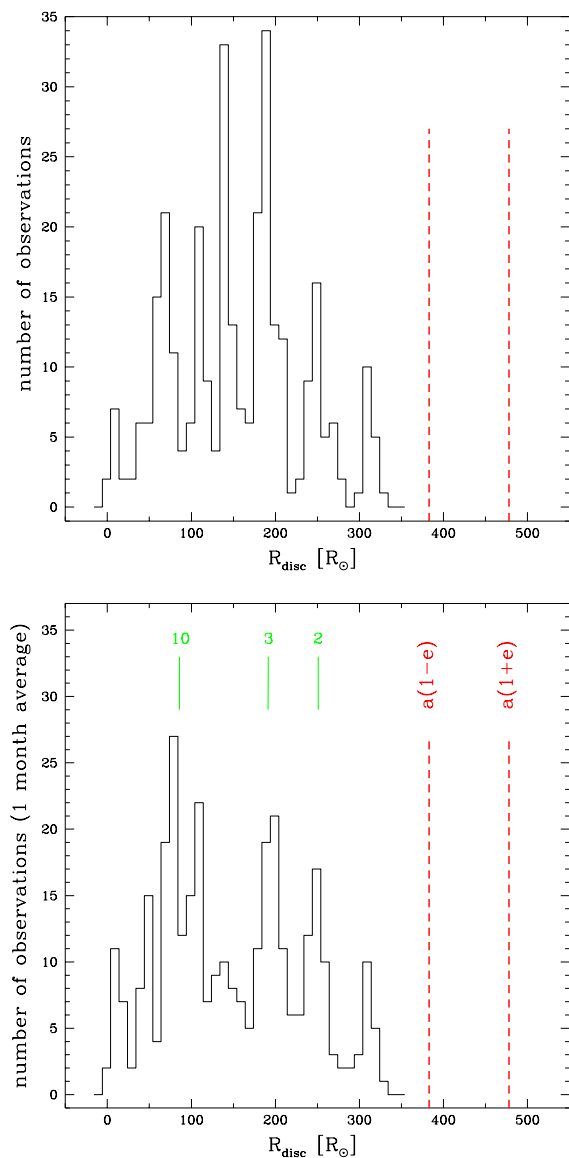


Fig. 4. Distribution of the calculated disc radius. The red dashed lines indicate the distance between components at periastron and apastron; the green solid lines show the resonances. The upper panel show the observed values; the lower indicate 30 days binned.

on the later spectrum this material emits in the central part of the line. Ring-like structures in Be discs are discussed for example by Struve (1931) and Rivinius et al. (2001). In X Per, Tarasov & Roche (1995) detected the appearance and development of an inner ring-like structure in the period 1993-1995, when the disc was starting to rebuilt after a disc-less phase.

Supposing that the variability seen on Fig. 3 represents a ring-like structure (a ring-like density enhancement) in the disc, we calculate that the ring initially emits at $\Delta V = 220 \text{ km s}^{-1}$, and later at $\Delta V = 78 \text{ km s}^{-1}$. Applying Eq.2 we obtain that the material moved from $40 R_{\odot}$ to $325 R_{\odot}$ for 447 days, having average outflow velocity 5.0 km s^{-1} . This velocity is about eight times faster than the velocity we estimated from disc build-up, and might be an indication that once the disc is developed the material can move faster inside the disc.

4.2. Disc truncation

The tendency for the disc emission fluxes to cluster at specified levels is related to the truncation of the disc at specific disc radii by the orbiting compact object (e.g. Coe et al. 2006). Okazaki & Negueruela (2001) proposed that these limiting radii are defined by the closest approach of the companion in the high-eccentricity systems and by resonances between the orbital period and disc gas rotational periods in the low-eccentricity systems. The resonance radii are given by

$$R_{n:m}^{3/2} = \frac{m (G M_1)^{1/2} P_{orb}}{2 \pi n}, \quad (4)$$

where G is the gravitational constant, n is the integer number of disc gas rotational periods, and m is the integer number of orbital periods. The important resonances are not only those with $n : 1$, but can as well be $n : m$ in general.

The histograms of $H\alpha$ disc size, R_{disc} , as calculated by Eq. 3, are plotted in Fig. 4. We use data for W α from Reig et al. (2016), Grundstrom et al. (2007), and Li et al. (2014), as well as data from Table 1. Fig. 4 (the upper panel) is the histogram of the measured values of R_{disc} . This histogram is affected by the distribution of the observations, for example if we have many observations in one month it could produce a spurious peak in the histogram. To correct for this effect we calculate the average values for each 30 day. If there is no data for a given interval, we interpolate between the nearest values. The 30-day binned values are plotted in Fig. 4 (lower panel). The 30-day bin was used because we do not detect variability in $H\alpha$ on a timescale shorter than 10 days, but we do detect variability on 60 days. Binning with 20 and 40 days provide very similar results. The comparison between Fig. 4a and Fig. 4b shows that the spurious effects due to unequal distribution of the observations are removed.

Fig. 4 is based on data over the last 26 years from 1992 to 2018. We note that in three X-ray/ γ -ray binaries (LSI+61 303, MWC 148, and MWC 656) the distribution of R_{disc} values has one very well-pronounced peak (Zamanov et al. 2016). In X Per we see a few peaks rather than a single peak. The most pronounced peaks correspond to 10:1, 3:1, and 2:1 resonances. In X Per it seems that in the beginning of the disc-rise the resonance 10:1 operates, after this more disc material appears, the disc grows, and the resonance 3:1 starts to operate, and later 2:1. A more or less similar situation is in the Be/X-ray binary V725 Tau / 1A 0535+262, where multiple resonances are discussed, i.e. 1:4, 1:5, and 1:7 (Coe et al. 2006). The orbital period of V725 Tau is 111.1 days (Finger et al. 1996). This similarity indicates that in such wide systems different resonances can operate probably depending on the mass loss of the primary and the development of its circumstellar disc.

Following Yatabe et al. (2018), we adopt $P_{orb} = 251.0 \pm 0.2 \text{ d}$ and mass of the neutron star $M_{ns} = 2.03 M_{\odot}$. For the primary we assume $M_1 = 13.5 M_{\odot}$ (see Sect. 3). With these values we calculate mass ratio $q = M_1/M_{ns} = 6.65$ and semi-major axis of the orbit $a = 418 R_{\odot}$. Using the formula by Eggleton (1983), we estimate the Roche lobe size of the primary $r_L = 228 R_{\odot}$. The orbital eccentricity of the system is low $e \approx 0.11$ (Delgado-Martí et al. 2001). The distance between components at periastron is $a(1-e) = 372 R_{\odot}$ and at apastron is $a(1+e) = 464 R_{\odot}$.

The maximum disc size observed in our data is $R_{disc} = 337 R_{\odot}$, which is smaller than the closest approach of the neutron star. However, it is larger than the size of the Roche lobe of the Be star, i.e. $r_L < R_{disc}(max) < a(1-e)$.

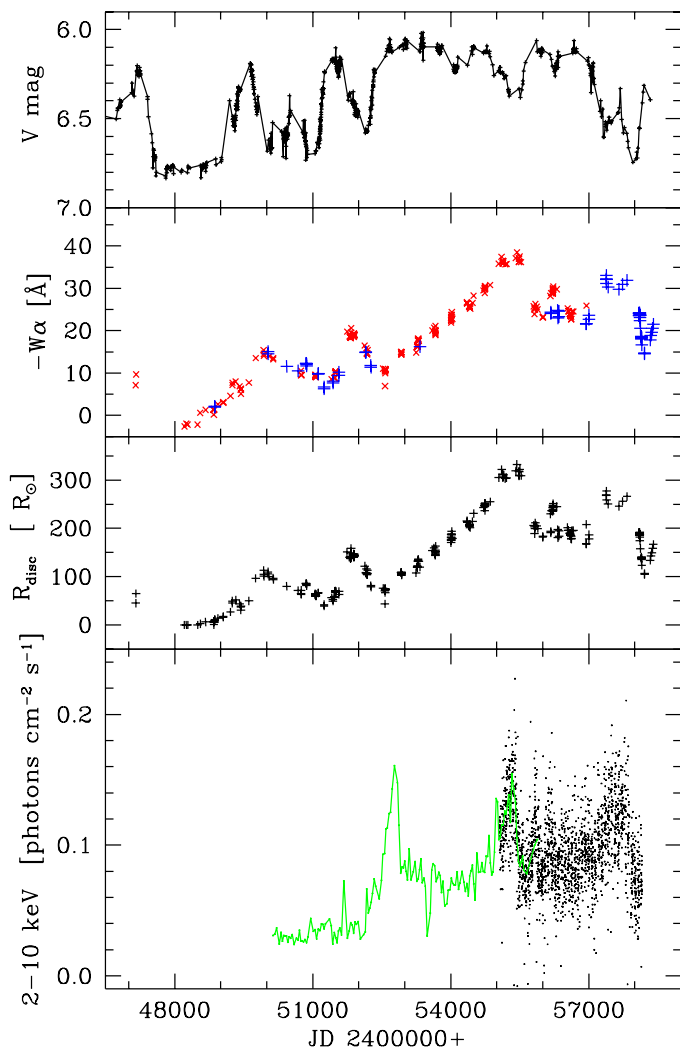


Fig. 5. X Per - connection between $H\alpha$ and X-ray variability. Shown from top to bottom are V-band magnitude, equivalent width of $H\alpha$ emission, circumstellar disc radius, and X-ray flux.

The Be/X-ray binaries present different states of X-ray activity (Stella et al. 1986; Negueruela 1998). X Per does not show periodic Type I outbursts, which are common feature in the classical Be/X-ray binaries and occur when a neutron star moving along an eccentric orbit crosses the Be circumstellar disc during the periastron passage. The result that $R_{disc(max)} < a(1 - e)$ demonstrates that the neutron star does not pass through the disc of the donor star even at the maximum disc size observed during the last 30 years. Periodic Type I outbursts in X Per can be expected if $W\alpha$ achieves the level of about 45 Å or above it.

4.3. Be disc \rightarrow X-ray flux

The mass transfer rate onto the neutron star and subsequent accretion-driven X-ray flux should depend on the changes in the radius of the disc of the Be star that we can track through the variations in $H\alpha$ emission line. The V-band magnitude, $W\alpha$, the calculated disc radius, and X-ray data are plotted in Fig. 5. The V-band data are from American Association of Variable Star Observers (AAVSO). The X-ray data are from

RXTE/ASM (Jahoda et al. 1996; Levine et al. 1996) and MAXI (Matsuoka et al. 2009). The RXTE/ASM X-ray light curve is rebinned with a time of 30 days and scaled relatively to the MAXI counts (binning with 25 or 35 days provide very similar light curve). In the panel $W\alpha$, the red crosses are data from the literature (Reig et al. 2016; Grundstrom et al. 2007; Li et al. 2014). The blue plus signs represent Rozhen, TIGRE, and ELODIE data from our Tables 1 and 2 of Zamanov et al. (2001).

Li et al. (2014) discussed the connection between $H\alpha$ and X-ray flux during the period JD 2451000 - JD 2455000. They pointed out the time delay between the $W\alpha$ maximum at about JD 2452000 and X-ray maximum, which is ~ 800 days later. They used this delay to estimate the viscosity in the outflowing disc (α parameter). We point that there is a similar time delay between a minimum in $W\alpha$ at JD 2452600 and a minimum in RXTE/ASM X-ray flux at JD 2453500.

After JD 2454000 $W\alpha$ increases and the X-ray flux also increases, which indicates that the neutron star accretes more material and probably truncates the outer parts of the disc. Two stronger peaks are visible in $W\alpha$ at JD 2455000 and JD 2457500. Both of these peaks are also well detectable in the MAXI X-ray data. We performed correlation analysis and found moderate to strong correlation between $W\alpha$ and X-ray flux with the Pearson correlation coefficient 0.61-0.66, Spearman's (ρ) correlation coefficient 0.61-0.68, and significance, p -value in the range $5 \times 10^{-6} - 1 \times 10^{-8}$. There is no time delay between $W\alpha$ and X-ray flux after JD 2454000. If a time delay exists it is less than 40 days.

A comparison between the behaviour of V brightness and $W\alpha$ shows that before JD 2453000 these parameters vary almost simultaneously – the maxima of $W\alpha$ correspond to the maxima of the V-band brightness and have time delays ≤ 300 days. After it, the behaviour is different – the maxima of $W\alpha$ and R_{disc} correspond to minima of the V-band brightness.

5. Discussion

For Be stars, Hanuschik et al. (1988) found that the peak separations of $H\alpha$ and $H\beta$ emission lines follow the relation $\Delta V_\beta = 1.8\Delta V_\alpha$. For X Per the ratio $\Delta V_\beta/\Delta V_\alpha$ is considerably below the average value for Be stars (see Sect. 4). At this stage considerable deviation from the behaviour of the Be stars is also detected in LSI+61⁰303 (Zamanov et al. 2016). In both star the $H\alpha$ -emitting disc is only 1.7 times larger than the $H\beta$ -emitting disc, while in normal Be stars it is 3.2 times larger. This can be a result of truncation of the outer parts or different density structures in the inner parts of the Be disc.

The pulse period of neutron star in X Per shows episodic spin-ups and spin-downs. Between 1972 and 1978 the neutron star has been spinning up with a rate of $\dot{P}/P \approx -1.5 \times 10^{-4} \text{ yr}^{-1}$ (Henrichs 1983). Since 1978 till 2002 the neutron star has been spinning down with a rate $\dot{P}/P \approx 1.3 \times 10^{-4} \text{ yr}^{-1}$. After 2002 (JD 2452000) a new episode of spin-up has began (Blay & Reglero 2012; Acuner et al. 2014). This new spin-up began together with the increase of the X-ray brightness, and its start corresponds to the moment when $W\alpha$ achieved 20 Å and $R_{disc} \approx 150 R_\odot$.

Yatabe et al. (2018) analysed X-ray data and estimated for the neutron star in X Per mass $M_{ns} = 2.03 \pm 0.17 M_\odot$, and magnetic field $B = (4 - 25) \times 10^{13} \text{ G}$, adopting GAIA distance $d = 810 \text{ pc}$. They also found that the X-ray luminosity varies in the range 2.5×10^{34} to $1.2 \times 10^{35} \text{ erg s}^{-1}$.

Postnov et al. (2017) proposed that in the enigmatic Be star γ Cassiopeia the elusive companion is a neutron star acting as a

propeller. In this scenario, the subsequent evolutionary stage of γ Cas and its analogues should be X Per-type binaries comprising low-luminosity slowly rotating X-ray pulsars. The corotation radius of the neutron star is

$$R_{co} = \left(\frac{G M_{ns} P_{spin}^2}{4 \pi^2} \right)^{1/3}. \quad (5)$$

The radius of its magnetosphere (the Alfvén radius) is

$$R_m = \frac{(B R_{ns}^3)^{4/7}}{\dot{M}_{acc}^{2/7} (2 G M_{ns})^{1/7}}. \quad (6)$$

In the standard theory of gravimagnetic rotators (Lipunov 1987; Campana et al. 2018) for a neutron star to be accretor (X-ray pulsar) the condition is that the magnetosphere radius should be smaller than the corotation radius, $R_m \leq R_{co}$. Assuming $R_{ns} = 10$ km and that X-ray flux is equal to the accretion luminosity,

$$L_{acc} = G M_{ns} \dot{M}_{acc} R_{ns}^{-1}, \quad (7)$$

we estimate that the mass accretion rate is in the range 1.47×10^{-12} to $7.07 \times 10^{-12} M_{\odot} \text{ yr}^{-1}$ (from 9.28×10^{13} to $4.45 \times 10^{14} \text{ g s}^{-1}$). We calculate that at low accretion rate $R_m \approx R_{co} \approx 0.24 R_{\odot}$, in other words at low X-ray flux the neutron star is close to the accretor-propeller transition boundary. The condition that the neutron star in X Per is an accretor (not propeller), $R_m \leq R_{co}$, also puts a limit on the magnetic field strength, $B \leq 1.15 \times 10^{14} \text{ G}$. This value is estimated taking into account the deviation of the magnetosphere radius from the the Alfvén radius (e.g. Bozzo et al. 2018). If the magnetic field is above this value, the neutron star would act as a propeller, the X-ray luminosity would decrease and the X-ray pulsations would disappear (which is not observed).

Roche et al. (1993) found a clear correlation between the optical, infrared, and X-ray behaviours during the 1974-1977 low state, followed by an extended period in which the X-ray behaviour appears to be unrelated to the optical. Li et al. (2014), analysing data obtained after the disc-less episode in 1990, found a time delay of about 800 days between $W\alpha$ and X-ray flux. This time delay exists before JD 2454000. After JD 2454000 (as visible on Fig. 5) there is no time delay, but there is a correlation between the variability of $W\alpha$ and X-ray flux. As the $W\alpha$ increases, the X-ray flux also increases. This is indicating a direct linkage between the circumstellar disc around mass donor and accretion rate onto the neutron star. This linkage is visible when $W_{\alpha} > 20 \text{ \AA}$ and $R_{disc} > 200 R_{\odot}$. When the circumstellar disc around the primary increases above $200 R_{\odot}$, the quantity of the material that is captured in the accretion cylinder of the neutron star also increases. The Roche lobe size of the primary is $r_L = 227 R_{\odot}$ (see Sect. 4.2). When $W_{\alpha} \approx 25 \text{ \AA}$, $R_{disc} \approx r_L$, the circumstellar disc fills the Roche lobe around the primary and the neutron star begins to accrete material from the Roche lobe overflow. In the past few years the existence of a relatively efficient mode of wind mass accretion in a binary system has been proposed, called the wind Roche lobe overflow (WRLOF; Mohamed & Podsiadlowski 2007), which lies in between the canonical Bondi-Hoyle-Littleton accretion and Roche lobe overflow. In case of X Per, most probably before JD 2454000 the circumstellar disc is small, it is well inside the Roche lobe ($R_{disc} < r_L$) and wind accretion (Bondi-Hoyle-Littleton accretion) is acting. After JD 2454000 when the circumstellar disc size achieves the Roche lobe, $R_{disc} \gtrsim r_L$, the

accretion mode changes to WRLOF, and the neutron star is accreting material directly from the circumstellar disc (Roche lobe overflow from the circumstellar disc) without time delay.

Other possibilities include the development of spiral arms (Grundstrom et al. 2007) or other large-scale perturbations (Negueruela et al. 1998) in the circumstellar envelope excited by tidal interaction which may lift disc gas out to radii where the accretion by the neutron star becomes more effective.

6. Conclusions

We present optical spectroscopic observations of the Be/X-ray binary X Per, optical counterpart of the X-ray pulsar 4U 0352+309. In this work, we combine published data with our measurements. First, we estimate, that the expansion velocity of the circumstellar disc is in the range $0.4 - 0.7 \text{ km s}^{-1}$. Second, we find that the distribution of the disc radius from the average equivalent width suggests resonant truncation of the disc, while the maximum disc radius is smaller than the separation of the stars at periastron but larger than the Roche lobe of the primary. Third, we derive a correlation between the equivalent width of $H\alpha$ emission line and X-ray flux, which is visible since JD 2454000, when $15 \text{ \AA} < W_{\alpha} \leq 40 \text{ \AA}$. We briefly discuss possible mechanisms of mass transfer.

Acknowledgements. This work is supported by the grant KII-06-H28/2 08.12.2018 (Bulgarian National Science Fund). It is based on observations from Rozhen National Astronomical Observatory, Bulgaria and the TIGRE telescope, located at La Luz, Mexico. TIGRE is a joint collaboration of the Hamburger Sternwarte, the University of Guanajuato and the University of Liège. This research has made use of (1) the MAXI data provided by RIKEN, JAXA, and the MAXI team; (2) results provided by the ASM/RXTE teams at MIT and at the RXTE SOF and GOF at NASA's GSFC; and (3) observations from the AAVSO International Database contributed by observers worldwide. UW acknowledges funding by DLR, project 50OR1701. DM acknowledges partial support by grants DN 08/20/2017 and RD-08-112/2018. We are very grateful to the referee whose comments helped to improve considerably the original manuscript.

References

- Acuner, Z., İnam, S. Ç., Şahiner, Ş., et al. 2014, MNRAS, 444, 457
Andrillat, Y. 1983, A&AS, 53, 319
Apparao, K. M. V. 1994, Space Sci. Rev., 69, 255
Blay, P. & Reglero, V. 2012, in Proceedings of “An INTEGRAL view of the high-energy sky (the first 10 years)” - 9th INTEGRAL Workshop and celebration of the 10th anniversary of the launch (INTEGRAL 2012). 15-19 October 2012. Bibliothèque Nationale de France, Paris, France. Published online at <http://pos.sissa.it/cgi-bin/reader/conf.cgi?confid=176>, id., 26
Boney, T., Markov, H., Tomov, T., et al. 2017, Bulgarian Astronomical Journal, 26, 67
Bozzo, E., Ascenzi, S., Ducci, L., et al. 2018, A&A, 617, A126
Braes, L. L. E. & Miley, G. K. 1972, Nature, 235, 273
Campana, S., Stella, L., Mereghetti, S., & de Martino, D. 2018, A&A, 610, A46
Catanzaro, G. 2013, A&A, 550, A79
Coe, M. J., Reig, P., McBride, V. A., Galache, J. L., & Fabregat, J. 2006, MNRAS, 368, 447
Dachs, J., Hanuschik, R., Kaiser, D., & Rohe, D. 1986, A&A, 159, 276
Dachs, J., Hummel, W., & Hanuschik, R. W. 1992, A&AS, 95, 437
de Loore, C., Altamore, A., Baratta, G. B., et al. 1979, A&A, 78, 287
Delgado-Martí, H., Levine, A. M., Pfahl, E., & Rappaport, S. A. 2001, ApJ, 546, 455
Doroshenko, V., Santangelo, A., Kreykenbohm, I., & Doroshenko, R. 2012, A&A, 540, L1
Dorren, J. D., Guinan, E. F., & McCook, G. P. 1979, IAU Circ., 3352
Eggleton, P. P. 1983, ApJ, 268, 368
Fabregat, J., Reglero, V., Coe, M. J., et al. 1992, A&A, 259, 522
Finger, M. H., Wilson, R. B., & Harmon, B. A. 1996, ApJ, 459, 288
Gaia Collaboration, Brown, A. G. A., Vallenari, A., et al. 2018, A&A, 616, A1
Gaia Collaboration, Prusti, T., de Bruijne, J. H. J., et al. 2016, A&A, 595, A1

- Grundstrom, E. D., Boyajian, T. S., Finch, C., et al. 2007, *ApJ*, 660, 1398
- Grundstrom, E. D. & Gies, D. R. 2006, *ApJ*, 651, L53
- Hanuschik, R. W. 1986, *A&A*, 166, 185
- Hanuschik, R. W. 1989, *Ap&SS*, 161, 61
- Hanuschik, R. W., Kozok, J. R., & Kaiser, D. 1988, *A&A*, 189, 147
- Henrichs, H. F. 1983, in *Accretion-Driven Stellar X-ray Sources*, ed. W. H. G. Lewin & E. P. J. van den Heuvel, 393–429
- Hohle, M. M., Neuhäuser, R., & Schutz, B. F. 2010, *Astronomische Nachrichten*, 331, 349
- Jahoda, K., Swank, J. H., Giles, A. B., et al. 1996, in *Proc. SPIE, Vol. 2808, EUV, X-Ray, and Gamma-Ray Instrumentation for Astronomy VII*, ed. O. H. Siegmund & M. A. Gummin, 59–70
- Knigge, C., Coe, M. J., & Podsiadlowski, P. 2011, *Nature*, 479, 372
- La Palombara, N. & Mereghetti, S. 2007, *A&A*, 474, 137
- Levine, A. M., Bradt, H., Cui, W., et al. 1996, *ApJ*, 469, L33
- Li, H., Yan, J., Zhou, J., & Liu, Q. 2014, *AJ*, 148, 113
- Lipunov, V. M. 1987, *The astrophysics of neutron stars*
- Lutovinov, A., Tsygankov, S., & Chernyakova, M. 2012, *MNRAS*, 423, 1978
- Lyubimkov, L. S., Rostopchin, S. I., Roche, P., & Tarasov, A. E. 1997, *MNRAS*, 286, 549
- Maitra, C., Raichur, H., Pradhan, P., & Paul, B. 2017, *MNRAS*, 470, 713
- Matsuoka, M., Kawasaki, K., Ueno, S., et al. 2009, *PASJ*, 61, 999
- Mohamed, S. & Podsiadlowski, P. 2007, in *Astronomical Society of the Pacific Conference Series, Vol. 372, 15th European Workshop on White Dwarfs*, ed. R. Napiwotzki & M. R. Burleigh, 397
- Monageng, I. M., McBride, V. A., Coe, M. J., Steele, I. A., & Reig, P. 2017, *MNRAS*, 464, 572
- Moultaka, J., Ilovaisky, S. A., Prugniel, P., & Soubiran, C. 2004, *PASP*, 116, 693
- Negueruela, I. 1998, *A&A*, 338, 505
- Negueruela, I. 2004, in *Revista Mexicana de Astronomia y Astrofisica Conference Series, Vol. 20, Revista Mexicana de Astronomia y Astrofisica Conference Series*, ed. G. Tovmassian & E. Sion, 55–56
- Negueruela, I., Reig, P., Coe, M. J., & Fabregat, J. 1998, *A&A*, 336, 251
- Nieva, M.-F. 2013, *A&A*, 550, A26
- Nikolov, Y. M., Zamanov, R. K., Stoyanov, K. A., & Martí, J. 2017, *Bulgarian Astronomical Journal*, 27, 10
- Norton, A. J., Coe, M. J., Estela, A., et al. 1991, *MNRAS*, 253, 579
- Okazaki, A. T. & Negueruela, I. 2001, *A&A*, 377, 161
- Pfahl, E., Rappaport, S., Podsiadlowski, P., & Spruit, H. 2002, *ApJ*, 574, 364
- Porter, J. M. & Rivinius, T. 2003, *PASP*, 115, 1153
- Postnov, K., Oskinova, L., & Torrejón, J. M. 2017, *MNRAS*, 465, L119
- Reig, P. 2011, *Ap&SS*, 332, 1
- Reig, P., Nersesian, A., Zezas, A., Gkouvelis, L., & Coe, M. J. 2016, *A&A*, 590, A122
- Rivinius, T., Baade, D., Štefl, S., & Maintz, M. 2001, *A&A*, 379, 257
- Roche, P., Coe, M. J., Fabregat, J., et al. 1993, *A&A*, 270, 122
- Roche, P., Larionov, V., Tarasov, A. E., et al. 1997, *A&A*, 322, 139
- Schmidt-Kaler, T. 1982, *Landolt-Börnstein. Numerical data and functional relationships in science and technology. New Series. Group VI: Volume 2/b*
- Schmitt, J. H. M. M., Schröder, K.-P., Rauw, G., et al. 2014, *Astronomische Nachrichten*, 335, 787
- Slettebak, A., Collins, II, G. W., & Truax, R. 1992, *ApJS*, 81, 335
- Stella, L., White, N. E., & Rosner, R. 1986, *ApJ*, 308, 669
- Struve, O. 1931, *ApJ*, 73, 94
- Taranova, O. G. & Shenavrin, V. I. 2017, *Astronomy Reports*, 61, 983
- Tarasov, A. E. & Roche, P. 1995, *MNRAS*, 276, L19
- Telting, J. H., Waters, L. B. F. M., Roche, P., et al. 1998, *MNRAS*, 296, 785
- van den Bergh, S. 1972, *Nature*, 235, 273
- Viotti, R., Ferrari-Toniolo, M., Giangrande, A., Persi, P., & Baratta, G. B. 1982, in *IAU Symposium, Vol. 98, Be Stars*, ed. M. Jaschek & H.-G. Groth, 423–426
- Worrall, D. M., Knight, F. K., Nolan, P. L., et al. 1981, *ApJ*, 247, L31
- Yatabe, F., Makishima, K., Mihara, T., et al. 2018, *PASJ*, 70, 89
- Zamanov, R. K., Reig, P., Martí, J., et al. 2001, *A&A*, 367, 884
- Zamanov, R. K., Stoyanov, K. A., Martí, J., et al. 2016, *A&A*, 593, A97
- Zamanov, R. K. & Zamanova, V. I. 1995, *Information Bulletin on Variable Stars*, 4189

Table 1. Spectral observations of X Per. The spectra marked with (*) are partly published in Zamanov et al. (2001).

file	telescope instrument	JD-start 2400000+	exp-time [min]	W_α [Å]	ΔV_α [km s ⁻¹]	ΔV_β [km s ⁻¹]
19920903*	2.0m Coude	48869.5278	59	-1.9	382	
19920905*	2.0m Coude	48871.5042	54	-2.2	386	
19951107.0024	Elodie	50029.4808	30	-14.9	177.8	202.0
19951107.0028	Elodie	50029.5449	45	-14.7	176.9	200.0
19961217.0024	Elodie	50435.3818	8	-12.1		
19970817*	2.0m Coude	50677.5447	15	-10.5	97	
19980209a*	2.0m Coude	50854.1816	5	-12.3	133	
19980209b*	2.0m Coude	50854.1856	5	-12.2	134	
19980219a*	2.0m Coude	50864.2089	7	-12.1	118	
19980219b*	2.0m Coude	50864.2191	7	-11.7	127	
19981102a*	2.0m Coude	51120.6553	15	-9.8	142	
19981102b*	2.0m Coude	51120.6660	15	-9.9	145	
19981230.65	2.0m Coude	51178.4811	25	-8.4	167.7	
19981230.66	2.0m Coude	51178.4991	25	-8.2	164.8	
19990309a*	2.0m Coude	51247.2356	20	-6.7	161	
19990309b*	2.0m Coude	51247.2497	20	-6.3	164	
19990919a*	2.0m Coude	51441.5191	20	-8.1	146	
19990919b*	2.0m Coude	51441.5333	10	-7.7	148	
20000129.0005	Elodie	51573.2545	30	-9.3	153.7	190.3
20000129.0006	Elodie	51573.2767	30	-10.0	153.6	193.5
20010903.178	2.0m Coude	52156.5933	10	-14.8	122	
20010903.179	2.0m Coude	52156.6006	8	-15.0	120	
20011220.0011	Elodie	52264.3216	30	-11.4		
20011221.0008	Elodie	52265.3375	60	-11.7		
20041117.0010	Elodie	53328.4980	33	-16.2	102.1	168.3
20120903.1	2.0m Coude	56173.5163	10	-24.08	—	
20120903.2	2.0m Coude	56173.5235	10	-24.41	—	
20130102.1	2.0m Coude	56295.3645	10	-25.61	81	
20130102.2	2.0m Coude	56295.3717	10	-25.95	88	
20130103.1	2.0m Coude	56296.3813	10	-26.39	85.9	
20130103.2	2.0m Coude	56296.3885	10	-26.54	85.8	
20141013.1	2.0m Coude	56944.4487	10	-24.4	105.5	
20141013.2	2.0m Coude	56944.4560	10	-24.17	101.8	
20141212.1	2.0m Coude	57004.4019	10	-26.8	87.2	
20141212.2	2.0m Coude	57004.4091	10	-26.6	108	
20151223.1	2.0m Echelle	57380.4701	30	satur.	—	144.0
20151223.2	2.0m Echelle	57380.4916	10	-36.4	—	146.7
20151224	2.0m Echelle	57381.3691	10	-36.3	—	145.3
20151226	2.0m Echelle	57383.3341	10	-36.1	—	145.1
20151227	2.0m Echelle	57384.3728	5	-36.5	—	145.2
20160130	2.0m Echelle	57418.2988	5	-33.9	95.3	124.9
20160923	2.0m Echelle	57654.5749	10	-30.8	—	143.3
20161211	2.0m Echelle	57734.3811	20	-32.7	63.0	133.5
20170317	2.0m Echelle	57830.2978	20	-30.9	—	126.1
20171207.1	2.0m Echelle	58095.2062	2	-23.5	119.4	
20171207.2	2.0m Echelle	58095.2107	15	-23.5	120.3	149.3
20171207.3	2.0m Echelle	58095.2226	15	-23.4	119.6	150.1
20171208.1	2.0m Echelle	58096.203	2	-22.7	117.8	
20171208.2	2.0m Echelle	58096.207	10	-23.5	121.8	148.0
20171220.2134	TIGRE	58108.6489	4	-25.0	125.3	
20171221.1853	TIGRE	58109.5373	4	-24.1	122.4	
20171222.1854	TIGRE	58110.5380	2	-23.4	120.3	
20171223.1922	TIGRE	58111.5571	4	-23.8	120.8	
20171224.1926	TIGRE	58112.5601	4	-23.0	120.7	
20171230	2.0m Echelle	58118.2314	20	-21.9	125.7	148.7
20180101	2.0m Echelle	58120.230	20	-19.8	121.5	143.7
20180103.1928	TIGRE	58122.5614	15	-20.5	122.2	
20180103.2156	TIGRE	58122.6638	15	-21.2	123.9	

Table 1. Continued.

20180104.0017	TIGRE	58122.7622	15	-20.2	124.1	
20180104.1921	TIGRE	58123.5563	15	-21.3	123.8	
20180105.1959	TIGRE	58124.5832	15	-21.1	121.9	
20180105.2219	TIGRE	58124.6805	15	-21.3	121.8	
20180106.0039	TIGRE	58124.7775	5	-20.7	121.3	
20180106.1923	TIGRE	58125.5582	15	-20.7	121.1	
20180106.2149	TIGRE	58125.6594	15	-21.0	121.0	
20180107.0014	TIGRE	58125.7601	15	-20.8	122.1	
20180126.01	2.0m Echelle	58145.2150	2	-18.34	106.3	
20180126.02	2.0m Echelle	58145.2170	3	-18.44	106.1	
20180126.03	2.0m Echelle	58145.2201	15	-18.05	106.8	
20180126.04	2.0m Echelle	58145.2312	20	-18.64	108.5	141.3
20180201.01	2.0m Echelle	58151.2218	20	-18.3	122.4	141.6
20180201.02	2.0m Echelle	58151.2312	5	-16.7	122.5	
20180402.01	2.0m Echelle	58211.2832	10	-14.7	105.8	115.0
20180402.02	2.0m Echelle	58211.2879	2	-14.5	103.6	
20180802	TIGRE	58332.9723	10	-17.83		
20180818	TIGRE	58348.9210	10	-18.89		
20180905	TIGRE	58366.8712	10	-19.62		
20180925	TIGRE	58386.8679	10	-20.61		
20181010	TIGRE	58401.8028	10	-21.51		